Received: 14 February 2019 | Revised: 2 April 2020 | Accepted: 27 April 2020

DOI: 10.1002/aoc.5823

Applied Organometallic Chemistry WILEY

FULL PAPER

X-ray structurally characterized Mo (VI), Fe (III) and Cu (II) complexes of amide-imine conjugate: (bio)catalytic and histidine recognition studies

Sabyasachi Ta[1] | **Milan Ghosh**[1] | **Noor Salam**[1] | **Jayanta Das**[1] | **Manirul Islam**[2] | **Paula Brandão**[3] | **Vítor Félix**[3] | **Jesus Sanmartin**[4] | **Debasis Das**[1]

[1]Department of Chemistry, The University of Burdwan, 713104, W, Burdwan, B, India

[2]Department of Chemistry, University of Kalyani, Kalyani, Nadia, 741235, India

[3]CICECO – Aveiro Institute of Materials, Department of Chemistry, University of Aveiro, Aveiro, 3810-193, Portugal

[4]Departamento de Química Inorgánica, Facultad de Química, Avda, Das Ciencias s/n, Santiago de Compostela, 15782, Spain

Correspondence
Manirul Islam, Department of Chemistry, University of Kalyani, Kalyani, Nadia, 741235, India.
Email: manir65@rediffmail.com

Vítor Félix, Department of Chemistry, CICECO – Aveiro Institute of Materials, University of Aveiro, 3810-193, Aveiro, Portugal.
Email: vitor.felix@ua.pt

Jesus Sanmartin, Departamento de Química Inorgánica, Facultad de Química, Avda. Das Ciencias s/n, 15782 Santiago de Compostela, Spain.
Email: jesus.sanmartin@usc.es

Debasis Das, Department of Chemistry, The University of Burdwan, Burdwan, 713104, W.B., India.
Email: ddas100in@yahoo.com

An amide-imine conjugate, (E)-N′-((2-hydroxybenzen-1-yl) methylene)-4-methylbenzohydrazide (H_2L^{PTASAL}), derived from 4-methyl-benzoic acid hydrazide (PTA) and 2-hydroxybenzaldehyde is used to prepare Mo (VI), Cu (II) and Fe (III) complexes. The X-ray structurally characterized complexes have been explored as catalyst for amine assisted asymmetric ring opening (ARO) of epoxide, carbon-heteroatom cross-coupling and ethyl benzene oxidation. In addition, their catecholase like activities have thoroughly been investigated. Moreover, the Cu (II) complex selectively recognizes histidine by fluorescence spectroscopy.

KEYWORDS

amide imine conjugate, catalysis, Fe (III) and cu (II) complexes, histidine recognition, Mo (VI)

1 | INTRODUCTION

Amide functionalities, the backbone of peptide[1] are present in ~25% drug molecules.[2] Both conformational diversity and stability allow amide derivatives as suitable

H2LPTASAL and their metal complexes 2 and 3 are deposited with CCDC numbers of 1834307, 1551324 and 1551323 respectively.

synthetic intermediates of stable functional materials.[2] Conventionally, amides are prepared by reaction of carboxylic acid derivative with appropriate amines.[3] Plethora of methods, *viz.* transition-metal and N-heterocyclic carbene (NHC) catalyzed[4,5] and oxidative amidation of aldehyde with amine[6–8] are worth mentioning.

It is well known that transition metal catalyzed asymmetric ring opening (ARO) of epoxide using varieties amines has unprecedented use for synthesis of bio-relevant, commercially significant, and enantiomerically pure β-amino alcohol.[9]

Moreover, transition-metal-catalyzed carbon–heteroatom cross-coupling reactions of phenols, amines and thiols with aryl halides leading to C-O, C-N and C-S bond formation have paramount importance for synthesis of bio-active compounds,[10] pharmaceuticals[11] and functional materials.[12] In spite of broad application of aryl sulfides in pharmaceutical industry, material science, and as organic intermediate, the carbon–sulfur bond formation have received relatively poor attention,[13] probably due to rapid and irreversible deactivation of the catalyst by sulfur species. In this context, copper-catalyzed Ullmann-type C–S cross coupling reaction is very relevant.[14]

Molybdenum complexes, precisely dioxomolybdenum (VI) complexes of N,O- donor hydrazide derivatives have interesting coordination chemistry[15] in terms of stereochemical and microelectronic properties. In addition to their impressive role in biotic processes, they possess potential catalytic activities.[16]

On the other hand, deviation from normal level of copper, involved in several bio-catalytic processes causes several diseases.[17–24] Copper complexes have potential antiviral, anti-bacterial and anti-tumor activities.[25] Several Cu (II) complexes have been used for trace level detection of varieties amino acids like histidine,[26] lysine,[27] cystine[28] and aspartic acid.[29] Deficiency of histidine, an essential amino acid for human growth and neurotransmitter[30] causes impaired nutritional state to patients having chronic kidney disease.[31,32] Therefore, easy detection and quantification of histidine in biological fluids is very demanding. The fluorescence method has advantage over other existing methods[33–35] in terms of sensitivity, inexpensive, simplicity, user friendly, instantaneous, invasive with direct visual perception.[36]

The essential red-ox active, iron regulates indispensable physiological functions including oxygen carrier in living organisms,[37] and is a cofactor of several enzymes.[38,39] Disturbance in cellular homeostasis causes labile iron to trigger uncontrolled Fenton reaction leading to peroxidative tissue damage causing several diseases, *viz.* Alzheimer's disease (AD), Parkinson's disease (PD) and various cancer.[40–42] It plays key role in oxygen metabolism and electron-transfer processes to DNA and RNA synthesis.[43,44]

Condensation of aromatic acid hydrazide with *o*-hydroxy benzaldehyde leads to H_2L^{PTASAL} (Scheme 1) having phenol-O, imine-N and amide-O donors. The HL^{PTASAL} binds Fe (III), Cu (II) and Mo (VI) to corresponding complexes *viz.* **$[Fe^{III}(HL^{PTASAL})(Cl)_2(OMe)](OH_2)$ (1)**, **$[Cu^{II}(HL^{PTASAL})(OH_2)_2](NO_3)$ (2)** and **$[Mo^{VI}(L^{PTASAL})(O)_2(OMe)]$ (3)** (Scheme 2). The Fe (III) complex **(1)** functions as an efficient, inexpensive catalyst for synthesis of β-amino alcohol *via* amine assisted ring opening of epoxide at room temperature.[45–48] The Cu (II) complex (**2**) can catalyze S-arylation *via* cross coupling between aryl halide and thiol. Moreover, it can selectively recognize histidine (His) through fluorescence spectroscopy. The Mo (VI) complex **(3)** catalyzes oxidation of ethyl benzene.

Thus, the present report indicates that a single ligand may combine at least three different metal ions tested, *viz.* Fe (III), Cu (II) and Mo (VI) to result three different complexes involving same donor sets irrespective of metal ion. All three metal complexes act as catalyst for targeted organic transformations. Interestingly, the Fe (III) complex that functions in aqueous medium has the potential to be a green catalyst.

2 | EXPERIMENTAL

2.1 | Materials

All experiments have been carried out in aerobic conditions. High-purity HEPES buffer, hydrazine hydrate, 3-methyl-1-benzoic acid, thionyl chloride and 2-hydroxy benzaldehyde are purchased from Sigma Aldrich (India). On the other hand, reagent grade metal salts like Cu

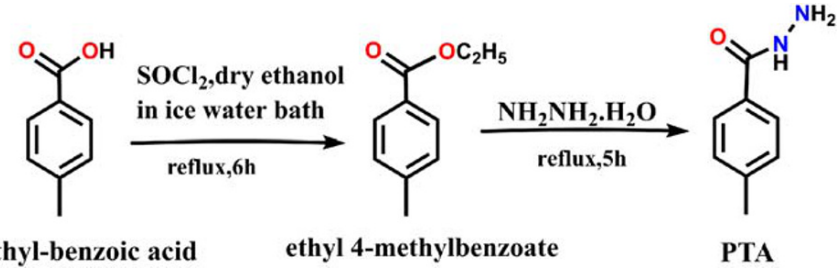

SCHEME 1 Synthesis of **PTA**

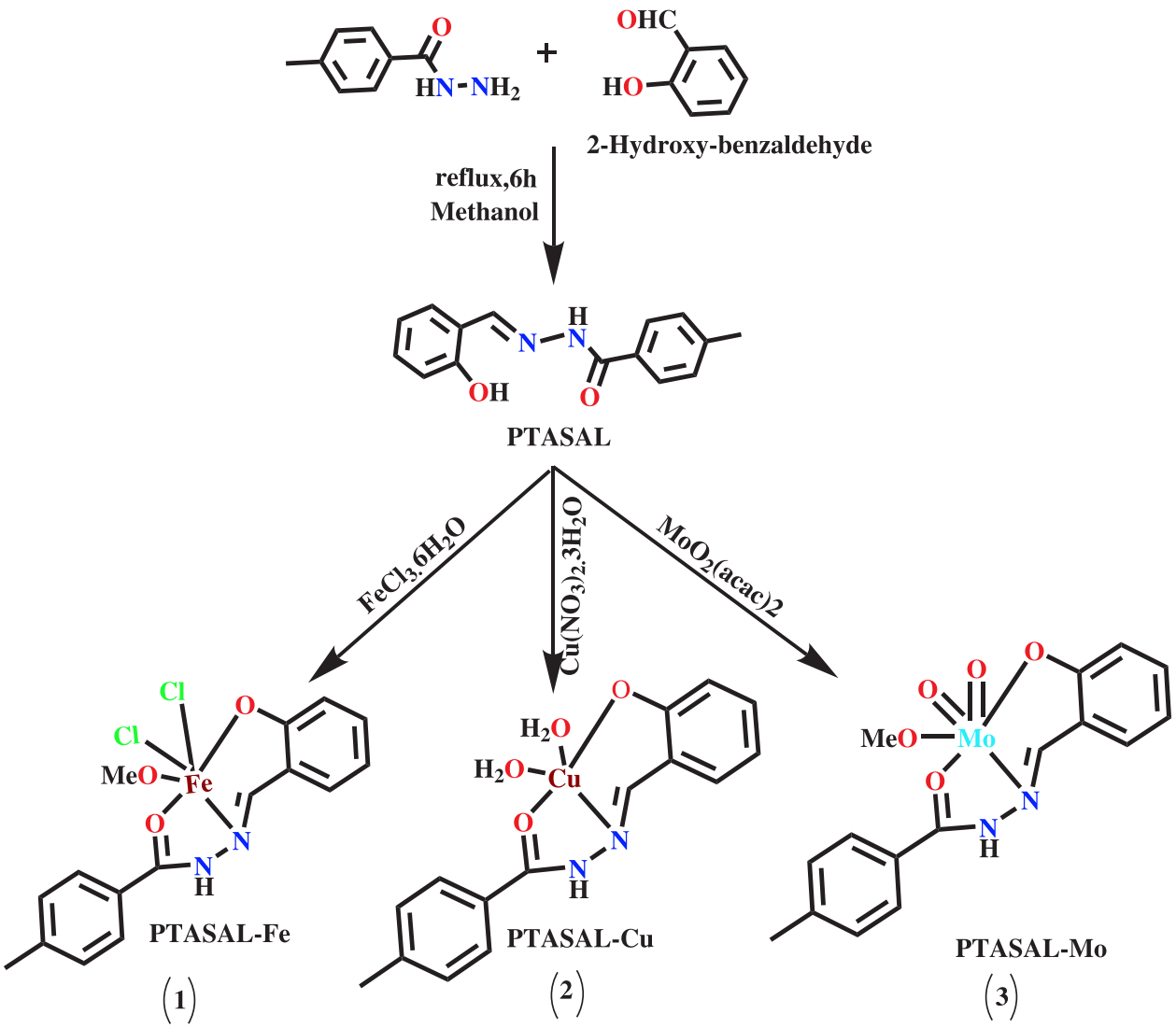

SCHEME 2 Synthesis of metal complexes of H_2L^{PTASAL}

$(NO_3)_2.3H_2O$, $FeCl_3.6H_2O$ and $MoO_2(acac)_2$ are purchased from Merck (India). Spectroscopic grade solvents have been used. Other analytical reagent grade chemicals have been used without further purification. Mili-Q Milipore 18.2 MΩ cm^{-1} water is used whenever required.

2.2 | Physical measurements

Elemental analyses have been performed with a PerkinElmer 2,400 series II CHN analyzer. FTIR spectra are recorded on a Shimadzu FTIR (model IR-Prestige 21 CE) spectrometer. The UV–vis. Spectra (1,000–240 nm) are collected with Shimadzu Multi Spec 2,450 spectrophotometer. The[1] H NMR and[13] C NMR spectra are measured with Bruker Advance 400 (400 MHz) and 300 (75 MHz) spectrometers. The steady state emission and excitation spectra are recorded with a Hitachi F-4500 spectrofluorimeter using 2.5 nm x 2.5 nm slit width. Systronics digital pH meter (model 335) and HCl/NaOH (50 μM) are used for measurement of pH. The cell path length for recording spectra is 1 cm. Electrospray ionization mass spectra (ESI-MS+) are recorded with a Thermo Fisher Scientific Exactive Plus mass spectrometer at a flow rate of 5 μL min^{-1} in spectroscopic grade methanol having compound concentration, 10^{-6} M. Varian 3,400 gas chromatography instrument equipped with 30 m CP-SIL8CB capillary column and FID is used for product characterization while a Trace DSQ II GC–MS equipped with a 60 m TR-50MS capillary column is used to confirm the products in catalysis studies. Thermal analyses have been performed with a

Mettler Toledo TGA/SDTA 851e and Perkin–Elmer Diamond TG/DT analyzer.

The single crystal X-ray diffraction data were collected on a Bruker X8 APEXII CCD diffractometer at 100 (2) K, using graphite-monochromatic Mo-K_α radiation (0.71073Å). Significant crystal parameters and refinement data are summarized in Table S1 (ESI). Data are processed and corrected for Lorentz and polarization effects. The structure of PATSAL was solved by standard direct methods[49] while the structures of its metal complexes were solved by intrinsic phasing.[50] Subsequently, they were refined by full matrix least squares on F.[251] All non-hydrogen atoms are anisotropic thermal parameters. Hydrogen atoms are included in the structure factor calculation in geometrically idealized positions with isotropic thermal displacements depending on the parent atom, using a riding model. Molecular diagrams were drawn with the Mercury [52] and PyMOL[53] software suites.

2.3 | Synthesis

2.3.1 | 4-methyl-benzoic acid hydrazide (PTA, Scheme 1)

At first, 4-methyl-benzoic acid is converted to acid chloride using thionyl chloride. The acid chloride is then treated with hydrazine to obtain PTA following literature method.[54] The ESI-MS(+), m/z, 151.60 and 173.65 are assigned to [PTA + H^+] and [PTA + Na^+] respectively (Figure S1, ESI). The ^{1}H NMR (Figure S2a, ESI, 400 MHz, DMSO-d_6, TMS, J (Hz), δ (ppm)): a, 9.698 (1H, s); b, 3.557 (2H, s); c, 2.320 (3H, s); aromatic proton, d, 7.695 (2H, d, J = 8) and e, 7.23 (2H, d, J = 8). ^{13}C NMR (Figure S2b, ESI, 400 MHz, DMSO-d_6): e, 166.24 (-$\underline{C}$ONHNH$_2$), f, 141.27 (-$\underline{C}$CH$_3$), g, 130.57 (-$\underline{C}_6$H$_4$), h, 129.11(-$\underline{C}$CONHNH$_2$), i, 127.15 (-$\underline{C}_6$H$_4$), j, 21.14 (-$\underline{C}$H$_3$). FTIR (Figure S3, ESI) (ν, cm^{-1}): 2821 ($\nu_{N\text{-}H}$), 2,970 ($\nu_{C\text{-}H}$ of CH$_3$), 1,657 ($\nu_{C=O}$).

2.3.2 | 4-Methyl benzoic acid-(2-hydroxy-benzylidene)-hydrazide (H_2L^{PTASAL}, Scheme 2)

A mixture of PTA (150 mg, 1 mmol) and 2-hydroxybenzaldehyde (122 mg, 1 mmol) in methanol is refluxed for 6 hr. Slow evaporation of the resulting solution produced X-ray quality needle shaped off-white crystals after several days. The yield is 70%. Anal. calcd. (%) for $C_{15}H_{14}N_2O_2$: C, 70.85; H, 5.55 and N, 11.02; found: C, 71.01; H, 5.27 and N, 11.47. ^{1}H NMR (Figure S4a, ESI, 400 MHz, DMSO-d_6), a, 11.792 (1H, s), CONH, b, 11.506 (1H, s), OH, c, 8.410 (1H, s), N=CH, d, 2.372 (3H, S), CH_3, 7.815 (2H, d, J = 8) and 7.326 (2H, d, J = 8) (aromatic ring protons from carboxylic acid moiety side), H, 7.178 (1H, d, J = 8.8), 6.116 (1H, d, J = 2.4), 6.116 (1H, d, J = 2.4), 6.919 (1H, m). ^{13}CNMR (Figure S4b, ESI, 400 MHz, DMSO-d_6), 162.55 (-$\underline{C}$ONH, e), 160.17 (-$\underline{C}$OH, f), 150.56 (-$\underline{C}$=N-, g), 142.19 (-$\underline{C}$CH$_3$, h), 132.09 (-$\underline{C}_6$H$_4$OH, i, ring carbon), 130.71 (-$\underline{C}$CONH-, j), 129.50 (-$\underline{C}_6$H$_4$CH$_3$, k, ring carbon), 127.95 (-$\underline{C}_6$H$_4$CONH-, l), 106.91 (m, ring carbon from aldehyde part), 104.08 (n, ring carbon from aldehyde part), 97.94 (o, ring carbon from aldehyde part), 21.50 (-$\underline{C}$H$_3$, p). ESI-MS(+) (Figure S5, ESI), m/z for [H_2L^{PTASAL} + CH_3OH + K^+], calcd. 327.09, found, 327. 41. FTIR data (Figure S6, ESI), 3,203 ($\nu_{N\text{-}H}$), 1,542 ($\nu_{C=N}$), 2,985 ($\nu_{C\text{-}H}$ of CH3); 1,635 ($\nu_{\text{-}C=O}$).

1. [Fe^{III}(HL)^{PTASAL})(C1)$_2$(MeOH)](OH)$_2$)

Methanol solution of $FeCl_3.6H_2O$ (0.061 g, 1 mmol, 5 ml) is added to the solution of H_2L^{PTASAL} (0.057 g, 1 mmol, 5 ml) in methanol under stirring condition. The stirring is continued for 30 min at room temperature (Scheme 2). After filtration, the filtrate is kept at room temperature for 5 days to obtain brown crystals with 70% yield. Anal. calcd. (%) for $C_{16}H_{18}Cl_2FeN_2O_4$: C, 44.79; H, 4.23 and N, 6.53; found: C, 43.37; H, 4.08 and N, 6.30. ESI-MS(+) (Figure S7, ESI), m/z for [**1** + CH_3OH + $Li]^+$, calcd. 469.06, found: 468.77; Selected FTIR data (cm^{-1}): 3413 ($\nu_{O\text{-}H}$), 3,152 ($\nu_{N\text{-}H}$), 1,597 ($\nu_{C=N}$), 3,040 ($\nu_{C\text{-}H}$ of CH3); 1,646 ($\nu_{C=O}$), (Figure S8, ESI). The UV–vis. Spectrum in aqueous methanol (1:1, v/v, 10 μM, Figure S9a, ESI): λ, nm (ε, M^{-1} cm^{-1}); 295 (7210). The TGA indicates that **1** undergoes decomposition in four stages (Figure S9b, ESI). At 108 °C, it loses water, at 201 °C it loses coordinated MeOH, at 374 °C it loses two Cl^- ion and at 768 °C HL^{PTASAL} unit exits from the complex. Finally Fe_2O_3 remains as residue.

2. [Cu^{II}(HL^{PTASAL})(OH$_2$)$_2$](NO$_3$)

Methanol solution of Cu $(NO_3)_2.3H_2O$ (190 mg, 1 mmol, 5 ml) is added to the solution of H_2L^{PTASAL} (200 mg, 1 mmol, 5 mL) in methanol under stirring condition. The stirring is continued for 1 hr (Scheme 2). Slow evaporation of solvent resulted intense green crystals after two days, suitable for X-ray diffraction. The yield is 81%. Anal. calcd. (%) for $C_{15}H_{17}CuN_3O_7$: C, 43.43; H, 4.13 and N, 10.13; found: C, 42.67; H, 4.01 and N, 9.30. ESI-MS($^+$) (Figure S10, ESI), m/z [Cu^{II} (^{t}HL^{PTASAL})(OH$_2$)$_2$](NO$_3$)$^+$ calcd. For $C_{15}H_{17}CuN_3O_7$: 414.05, found: 413.64; FTIR (ν, cm^{-1}): 3424 ($\nu_{O\text{-}H}$), 3,250 ($\nu_{N\text{-}H}$),1,604 ($\nu_{C=N}$), 3,059($\nu_{C\text{-}H}$ of CH3); 1,655 (C=O), (Figure S11, ESI). Absorption spectrum, λ_{max}/nm (ε_{max}/

M^{-1} cm^{-1} in MeOH): 285 (4034), 316 (2620), 395 (670), (Figure S12, ESI).

3. $[Mo^{VI}(L^{PTASAL})(O)_2(MeOH)]$

Methanol solution of $MoO_2(acac)_2$ (157 mg, 1 mmol, 5 ml) is added slowly to the solution of H_2L^{PTASAL} (93 mg, 1 mmol, 5 ml) in methanol under stirring condition and stirring is continued for 40 min (Scheme 2). The solution is allowed for slow evaporation while orange-yellow crystals are found after 5 days. The yield is 80%. Anal. calcd. (%): C, 46.62; H, 3.91 and N, 6.80; found: C, 46.90; H, 4.05 and N, 7.15. ESI-MS (Figure S13, ESI) (m/z): for $C_{16}H_{17}MoN_2O_5^+$ calcd. 413.28; found, 413.65, $C_{16}H_{16}MoN_2O_5Na^+$ calcd. 436.27; found, 436.75. ^{1}H NMR (Figure S14a, 400 MH_Z, $CDCl_3$): c, 8.677 (1H, s, N=CH), 7.875–7.855 (1H, d, J = 8.0 Hz), 7.728 (1H, s), 7.7088 (2H, s), 7.374–7.371 (3H, d, J = 0.6 Hz), 7.213 (1H, s), e, 3.494 (3H, s), $MoOCH_3$; d, 2.394–2.353 (3H, t, J = 8.2 Hz), CH_3; ^{13}CNMR (Figure S14b, 400 MHz, DMSO-d_6): g, 169.33, h, 153.59, i, 149.04, j, 136.73, k, 132.83, l, 130.47, m, 129.42, n, 128.24-, o, 108.41, p, 104.78, q, 97.94, r, 25.46 and s, 18.47. FTIR data (cm^{-1}): 3162 ($\nu_{N\text{-}H}$), 2,919 ($\nu_{C\text{-}H}$ of CH3); 1,651 ($\nu_{C=O}$), 1,597 ($\nu_{C=N}$) (Figure S14c, ESI). UV–vis. Spectrum (in MeOH, Figure S15, ESI) (ε_{max}/ M^{-1} cm^{-1}), 295 (10800); 316 (9840); 399 (2350).

3 | RESULTS AND DISCUSSION

3.1 | Single crystal X-ray structures of H_2L^{PTASAL} and its metal complexes.

The crystal structure of free ligand H_2L^{PTASAL}, is built-up from an asymmetric unit composed of two independent molecules, self-assembled by an almost linear hydrogen bond between the hydrazine proton and a carbonyl group from adjacent molecules, leading to the formation of a dimer entity. This directional bonding interaction has a N···O distance of 2.8084(15)Å and a N-H···O angle of 166.1(17)°. Moreover, the perspective view of the asymmetric unit, presented in Figure 1, shows that one molecule is planar while the other one, the phenyl substituent adjacent to the carbonyl group is rotated by 32.1(14)° relative to remaining planar ligand backbone. These two conformations are stabilized in solid state by a O-H···N intra-molecular hydrogen bond between phenol OH group and imine acceptor binding site, with O(12)···N(12) and O(22)···N(22) distances of 2.5982(15) and 2.5751(15)Å, respectively and corresponding O-H···N angles of 149.1(19) and 150.7(15)°. In crystal packing, the dimer entities are further connected by N-N-H···O hydrogen bonds with N···O [x, y-1, z] distance of 2.9390(15)Å and ∠N-H···O of 163.6(15)°, affording 1-D network of hydrogen bonds. Selected bond lengths in the metal coordination spheres of Cu (II) (**2**) and Mo

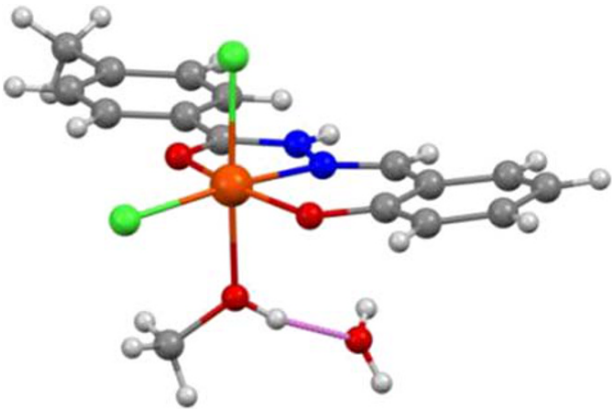

FIGURE 2 A ball and stick view of the asymmetric unit of $[Fe^{III}(HL^{PTASAL})Cl_2(MeOH)].H_2O$ (**1**)

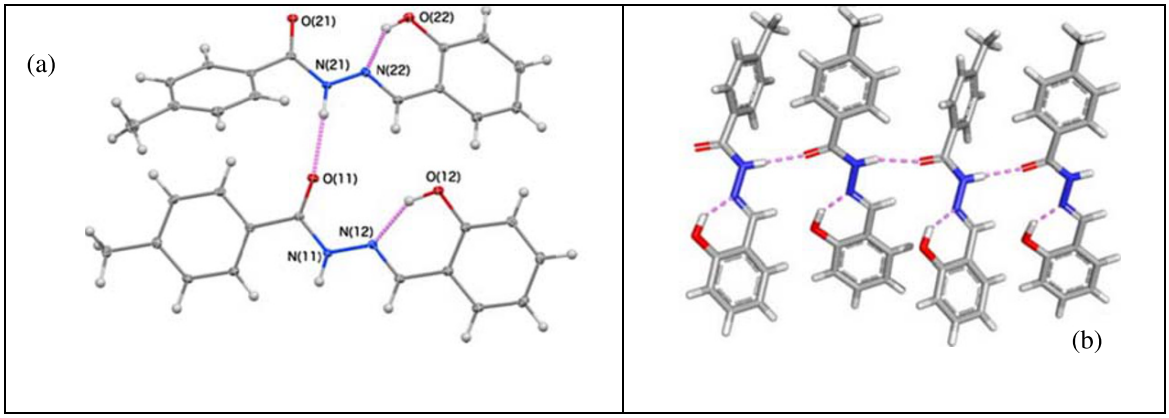

FIGURE 1 Crystal structure of H_2L^{PTASAL}: a) perspective view of asymmetric unit composed of two independent molecules having 30% thermal ellipsoid probability with relevant atom notation scheme; b) 1-D network of N-N-H···O hydrogen bonds

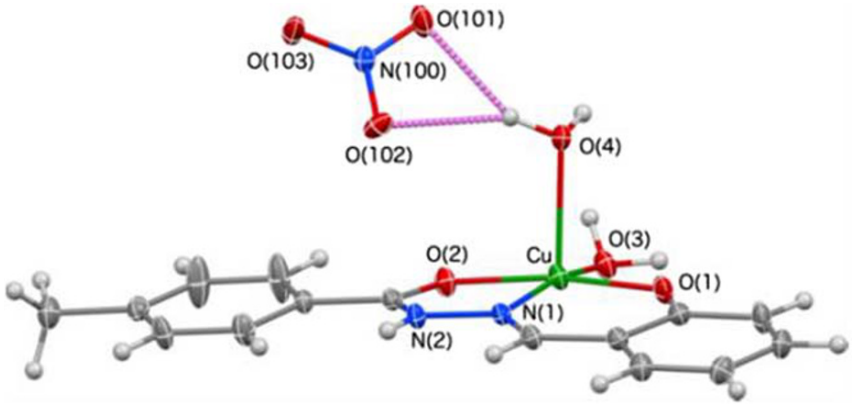

FIGURE 3 A perspective view of the asymmetric unit of $[Cu^{II}(HL^{PTASAL})(OH_2)_2](NO_3)$ having 30% thermal ellipsoid probability. The complex cation establishes with nitrate counter ion a bifurcate hydrogen bond

(VI) (**3**) complexes of H_2L^{PTASAL} are listed in Table S2 (ESI).

In spite of several attempts for a suitable crystal of **1**, very weak X-ray diffraction pattern lead to high R_1 value (*ca.* 0.13) that prevents its publication with detailed structural parameters. However, the molecular formula $[Fe^{III}(HL^{PTASAL})Cl_2(MeOH)].H_2O$ is equivocally revealed, being consistent with the mass spectra and elemental analysis data. The charge balance of neutral dichloro Fe (III) complex seeks single deprotonation of H_2L^{PTASAL}, where the phenoxido formation is more likely relative to dissociation of a hydrazinyl proton. The geometric arrangement of HL^{PTASAL} around Fe (III) center (Figure 2) is equivalent to $[Mo^{VI}(L^{PTASAL})(O)_2(MeOH)]$ with *cis*-oxo groups replaced by two chloride ligands described *infra*.

The perspective view of asymmetric unit of **2** presented in Figure 3, shows five coordinated complex, $[Cu^{II}(HL^{PTASAL})(OH_2)_2]^+$ interacting with nitrate counter ion *via* a bifurcate hydrogen with coordinated water molecule (N···O distances = 2.984 (4) and 3.042(3)Å and corresponding N-H···O angles of 150 and 151°). Tridentate chelating H_2L^{PTASAL} adopts planar conformation. The coordination geometry around Cu (II) center is distorted square pyramid characterized by an index structural parameter τ of 0.09 given by the formula $\tau = (\alpha-\beta)/60$,[55] where α and β are the angles O(1)-Cu-O (2) (170.80(10)°) and N(1)-Cu-O (4) (165.60(11)°) respectively. The τ parameter assumes values of 0 and 1 for perfect square pyramidal and bipyramidal coordination shapes respectively. Thus, imine nitrogen N (1) and two oxygen, O(1) and O(2) from H_2L^{PTASAL} define the basal plane together with an oxygen O(3) of a water molecule at Cu-O distance of 1.959(2)Å. The apical position is occupied by an a oxygen, O (4) from second water molecule at Cu-O bond distance of 2.281(2)Å, which is longer than the former, as expected for a d^9 Cu (II) center. The Cu-N and Cu-O bond distances are within the expected values.

In the crystal packing of **2**, one-dimensional chains composed of $[Cu^{II}(HL^{PTASAL})(OH_2)_2]^+$ cations and nitrate counter ions are linked by complex network of N-H···O and O-H···O hydrogen bonds (Figure 4). The most prominent structural feature of these pillars is the existence of centro-symmetric motifs, in which adjacent $[Cu^{II}(HL^{PTASAL})(OH_2)_2]^+$ cations are linked by six concomitant HO-H···O hydrogen bonds between water molecules leading to the formation of a $\{Cu_2O_2(H_2O)_4\}$ cubane central core (Figure 4b). The dimensions of hydrogen

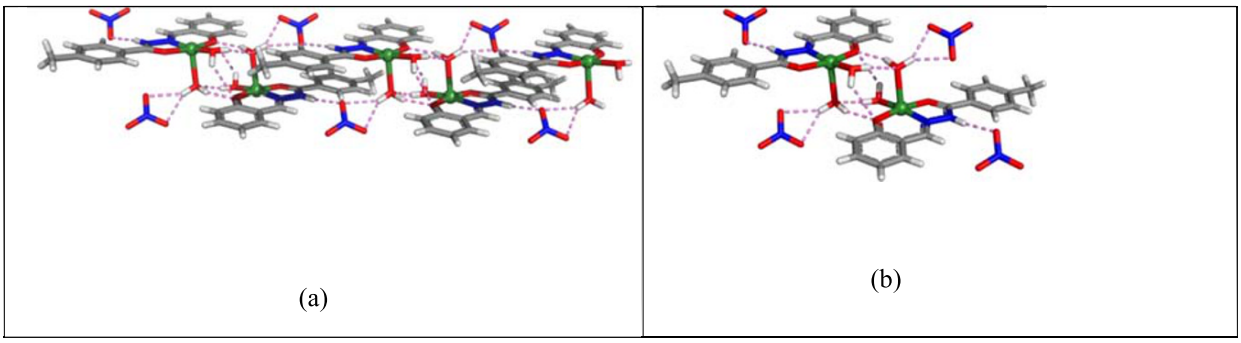

FIGURE 4 Crystal packing features of **2**: a) 1-D network of hydrogen bonds between $[Cu^{II}(HL^{PTASAL})(OH_2)_2]^+$ cations and nitrate counter ions with H_2L^{PTASAL} adopting a parallel disposition suggesting existence of π-π interactions; b) centro-symmetric arrangement of two complex cations with the formation of a central $\{Cu_2O_2(H_2O)_4\}$ motif derived from six O-H···O concomitant hydrogen bond interactions

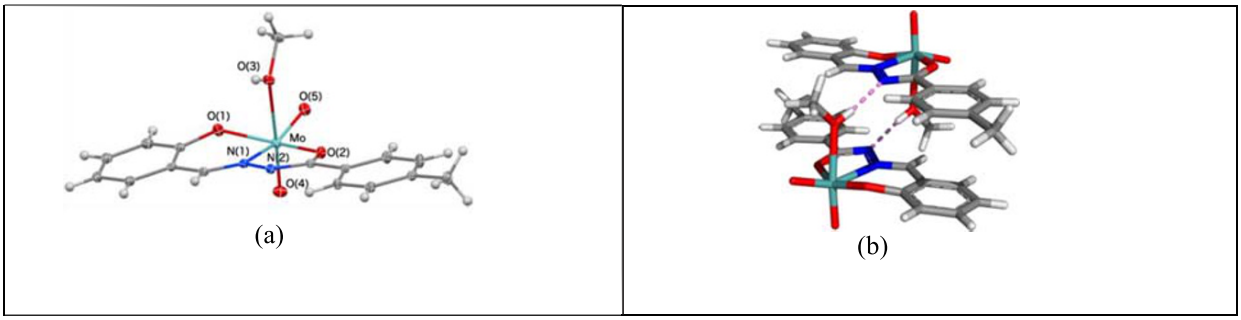

FIGURE 5 Crystal structure of **3**: a) perspective view of asymmetric unit with relevant atomic notation scheme having 30% thermal ellipsoid probability; b) centro-symmetric disposition of two [Mo^{VI} (L^{PTASAL})$(O)_2$(MeOH)] units self-assembled by two O-H···O hydrogen bonds

bonds found in the crystal structure are summarized in Table S3 (ESI). Moreover, the H_2L^{PTASAL} adopts a parallel disposition with phenyl and methylphenyl rings at centroid-centroid distance of 3.89 Å consistent with the existence of π-π interactions.

A molecular view of **3** depicted in Figure 5, shows a neutral complex consistent with molecular formula [Mo (L^{PTASAL})O_2(MeOH)] and two oxo groups adopting a *cis* spatial disposition. The charge balance of this Mo (VI) complex, requires protonation of non-coordinated imine nitrogen or oxygen atom of coordinated methanol. In agreement, in the final structure refinement one hydrogen atom is alternatively attached at geometric positions to the oxygen O(3) (model A) or nitrogen N (2). The trial refinement in model A gave lower wR_2 value than model B (0.0564 *versus* 0.0622). Therefore, the proton is definitively assigned to the coordinated MeOH and consequently the imine nitrogen of H_2L^{PTASAL} is non-protonated with a net charge of −1. The geometry around the Mo (IV) is a distorted octahedron with the imine nitrogen, N(1) and two oxygen donors, O(1) and O (2) from tridentate H_2L^{PTASAL} together with an oxo group, O(5) defining the equatorial plane. The axial positions are fulfilled with oxygen atoms, O(4) and O(3) from the second oxo-group and methanol respectively. The corresponding O(3)-Mo-O(4) angle, 171.74 (6)° is only 8.6° away from the axial coordination angle for a perfect octahedron (180°). Two terminal oxo groups, adopting a *cis* spatial disposition (∠O(4)-Mo-O (5) = 106.11 (7)°), exhibit typical Mo = O double bond distances of 1.6968 (14)Å and 1.7021(14)Å.[56,57] On the other hand, the longest bond observed in the metal coordination sphere is the Mo-O single bond, 2.3734(13)Å with coordinated MeOH. Furthermore, the selected bond distances and angles subtended at the metal center, listed in Table S8-S9 (ESI), agrees well with those reported for the octahedral complex [Mo(L)O_2(EtOH)][58] where L is a tridentate ligand analogue of H_2L^{PTASAL}.

In the crystal structure of **3,** the hydrogen atom molecules are self-assembled into centro-symmetric dimers *via* two almost linear N···H-O hydrogen bonds (N···O = 2.747 (2) Å; ∠ O-H···N*N* = 173.8(17)°), established between adjacent methanol and imine groups as depicted in Figure 5. Moreover, the phenyl rings of H_2L^{PTASAL} are π-π stacked in this centro-symmetric arrangement at centroid-centroid distance, 3.61 Å.

3.1 | Catalytic activity studies

3.1.1 | Synthesis of β-amino alcohol *via* epoxide ring opening (ERO)

The catalytic activity of **1** is explored by amine assisted ring opening of epoxide leading to β -amino alcohol at room temperature under solvent free condition (Scheme 3).

Room temperature synthesis of β-amino alcohol using aniline and styrene oxide *via* ERO reaction is chosen as model reaction. Probably labile chloride (Cl^-) in **1** is responsible for its catalytic activity that generate the required active site.[59] Table 1 shows the effect of different parameters like solvent, catalyst load and reaction time on product yield. The catalytic efficiency of **1** is the highest under solvent free condition at room temperature. With 15 mg catalyst load, 95% product yield is observed within 3 h. Various epoxides, *viz.* allyl glycidyl

SCHEME 3 Synthesis of β-amino alcohol at room temperature using **1** as catalyst

TABLE 1 Optimization of reaction parameters for synthesis of β-amino alcohol[a]

Entry	Catalyst load (mg)	Solvent	Time (h)	Yield[b] (%)
1.	None	None	24	--
2.	20	DCM	6	79
3.	20	H_2O	6	85
4.	20	Toluene	6	61
5.	20	None	6	95
6.	15	None	6	95
7.	15	None	5	95
8.	**15**	**None**	**3**	**95**
9.	10	None	3	72

[a]reaction conditions: aniline (1 mmol), styrene oxide (1 mmol), RT
[b]isolated yield of β-amino alcohol.

ether, epichlorohydrin, 1, 2-epoxy-3-phenoxy propane, cyclohexene oxide, styrene oxide and substituted anilines are subjected to ERO under optimized reaction conditions. The results are summarized in Table 2. In most cases, the reactions are completed within 3-6 h with reasonable yield. Styrene oxide and aryloxy epoxides undergo ERO by aniline through regioselective pathway with facile attack at less-hindered terminal carbon or benzylic carbon respectively (Table 2, entries 1 and 3). Meso epoxide like cyclohexene oxide provides corresponding amino alcohol with aromatic anilines with 90% yield (entry 2). Moreover, allyl glycidyl ether undergoes region-selective cleavage by aniline through less hindered carbon with moderate yield (Table 2, entry 4). Scheme 4 shows a proposed mechanism of ERO with epichlorohydrine (Table 2, entry 5) by aniline. Furthermore, ERO reaction involving substituted anilines having electron-withdrawing group and epichlorohydrin require higher time than aniline (Table 2, entry 6).

3.1.2 | Aryl-sulfur coupling between thio-phenol and aryl iodide.

Aryl-sulfur coupling reactions leading to diaryl sulfides have received considerable interest in biological, medicinal and material chemistry research. Here, **2** have been explored as catalyst for C-S cross-coupling reaction involving thiophenol and aryl iodide in water using K_2CO_3 as mild base at 90 °C (Scheme 5).

The **2** catalyzed S-arylation of thiophenol by iodobenzene is monitored as model reaction. Different factors governing the performance of **2** catalyzed cross coupling reactions are summarized in Table 3. Interestingly, the yield of the product is highest (98%) in aqueous medium (Table 3, Entry 3). Among various organic and inorganic bases tested like K_2CO_3, Cs_2CO_3, KOH and Et_3N, the efficiency of K_2CO_3 is highest in terms of product yield.

Varieties aromatic thiols and aryl halides are reacted under optimum conditions (Table 4). The reactions are very clean and smooth with moderate to good yield. Interestingly, aryl iodides having electron withdrawing group are more reactive than those having electron donating group. The nature of halogen affects the efficiency of the coupling reaction. The reactivity of different halo-benzenes are of the order iodobenzene > bromobenzene > chlorobenzene.

3.2 | Oxidation of ethyl benzene to acetophenone

The selective oxidation of ethyl benzene to acetophenone has been achieved under atmospheric pressure using 3 as catalyst (Scheme 6).

TABLE 2 ERO reaction between substituted amine and epoxide using **1** as catalyst[a]

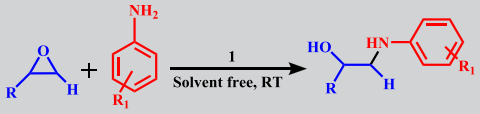

Entry	Epoxide	Amine	β-Amino alcohol	Time (h)	Yield[b,c] (%)
1	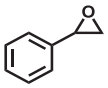		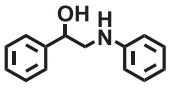	3	95
2			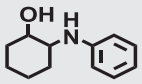	3	90
3	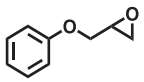		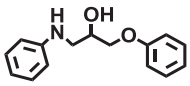	3	93
4	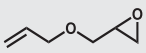		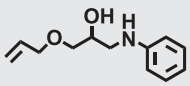	4	89
5	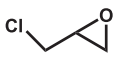		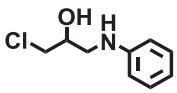	5	92
6	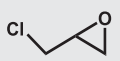	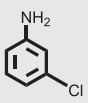	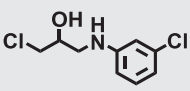	6	81

[a]**reaction condition:** epoxies (1 mmol), amine (1 mmol), 1 (15 mg), RT, solvent-free
[b]isolated yield
[c]products characterized by NMR (Fig.S16-S20, ESI).

The effect of several oxidants like TBHP, H_2O_2, PhIO, $NaIO_4$ and $KHSO_5$ on selective oxidation of ethyl benzene catalyzed by **3** is summarized in Table 5 (Entries 1–4). This is notable that TBHP has the best catalytic activity and good compatibility with reactants. Oxidants like H_2O_2, PhIO and $NaIO_4$ are less efficient than TBHP as evident from conversion percentage of ethyl benzene (Table 5, Entries 2–4). The use of $KHSO_5$ is excluded because a buffer is needed (Table 5, Entry 6).

The effect of temperature on the performance of the catalyst have been studied at three different temperatures, *viz.* 50, 60 and 70 °C (Table 5, entries 5–7). The maximum conversion (86%) is achieved at 60 °C. Although, at 70 °C, the initial conversion of ethyl benzene is higher than that observed at 60 °C,

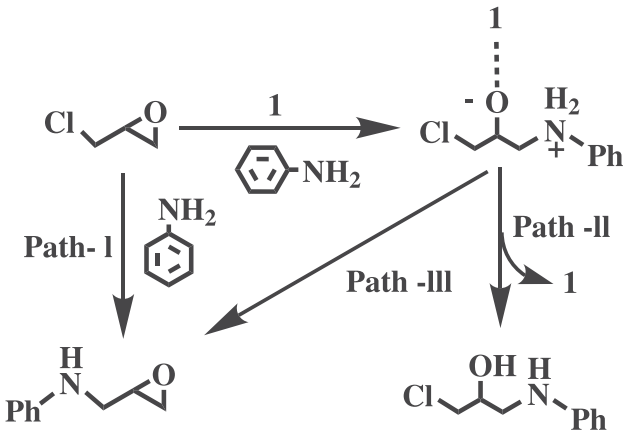

SCHEME 4 Proposed mechanism of ERO of epichlorohydrine by aniline

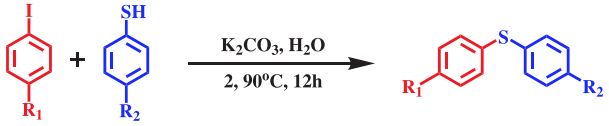

SCHEME 5 The C-S cross coupling reaction between thiophenol and aryl iodide

however as the reaction progress, the conversion is almost same to that observed at 60 °C. Therefore, optimum temperature for ethyl benzene oxidation is set to 60 °C.

A comparative table of three catalytic reactions *viz.* ERO, C-S coupling and ethyl benzene oxidation has been presented in ESI (Table S10).

3.3 | Recognition of histidine

Photo-physical interaction studies of **2** with natural amino acids have been studied in aqueous medium. The significant influence of His on the emission profile of **2** at pH 6–12 (Figure S21, ESI) insisted to perform the entire recognition studies at physiological pH, 7.4 using HEPES buffered aqueous methanol (0.1 M, MeOH/water, 9/1, *v*/v).

The change in UV–vis. Spectra of **2** upon gradual addition of His is shown in Figure 6a. The absorbance at 395 nm and 317 nm gradually weakens with the appearance of a new band at 332 nm signifying their interaction (Scheme 7). The changes in the absorption spectra of **2** in presence of different amino acids are shown in Figure 6b. The color change that occurs out of this interaction is due to liberation of free H_2L^{PTASAL} as His extracts out Cu^{2+} from the **2** forming [Cu (II)-His] complex (Scheme 7).

The fluorescence response of **2** towards other natural amino acids, *viz.* (1) Methionine, (2) Argenine, (3) Valine, (4) Leucine, (5) Serine, (6) Lysine, (7) Trptophan, (8) Phenylalanyl, (9) Glycine, (10) Glutamic acid, (11) Glutamine, (12) Proline, (13) Iso-leucine, (14) Asparagine, (15) Aspartic acid, (16) Tyrsosine, (17) Threonine, (18) Cystine and (19) Alanine is presented in Figure S22 (ESI). This indicates non-responsive nature of **2** towards other amino acids. In presence of His, the weak emission of **2** at 341 nm is red shifted to 357 nm (λ_{ex} = 297 nm, Φ = 0.0076) that steadily increase with increasing His concentration (Figure 7a). The emission intensity of **2** (λ_{em} = 357 nm) varies linearly with His concentration, the inset of which is useful for determination of unknown His concentration (Figure 7b).

The ESI-MS spectrum of the mixture of **2** and His supports the formation of [Cu (II)-His] complex (Figure S23, ESI), corroborated by its FTIR spectrum (Figure S24, ESI). The binding constant and lowest

TABLE 3 Effect of base and solvent on efficiency of **2** catalyzed C-S cross coupling reaction[a]

Entry	Base	Solvent	Yield (%)[b]
1	K_2CO_3	DMSO	73
2	K_2CO_3	DMF	86
3	K_2CO_3	H_2O	98
4	Cs_2CO_3	H_2O	82
5	KOH	H_2O	58
6	Et_3N	H_2O	34
7	Pyridine	H_2O	12
8	None	H_2O	None

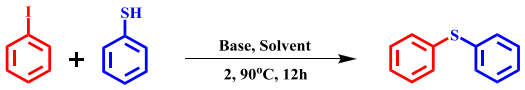

[a]Reaction condition: Iodobenzene (1 mmol), thiophenol (1.1 mmol), water (3 mL), base (2 mmol), **2** (15 mg), Temp.: 90 °C, Time: 12 h
[b]yield is determined by GC and GCMS analysis.

TABLE 4 The C-S cross coupling reaction involving various substrates using **2** as catalyst[a]

Entry	ArI	Ar-SH	Products	Yield (%)[b]	Yield[c]
1			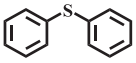	98	95
2	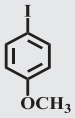		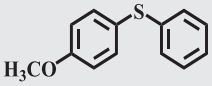	70	66
3	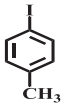		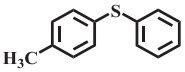	81	75
4	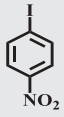		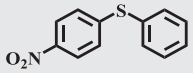	89	82
5			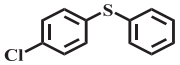	38	33
6			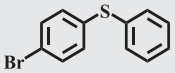	91	84
7			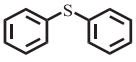	60	53
8			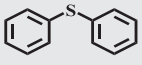	39	36
9	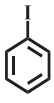	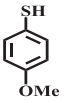	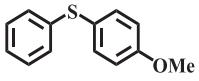	70	64

[a]**Reaction conditions:** aryl iodides (1 mmol), thiophenol (1.1 mmol), water (3 mL), K_2CO_3 (2 mmol) and **2** (15 mg), temp.: 90 °C, Time: 12 h.
[b]yield determined by GC analysis.
[c]isolated yield.

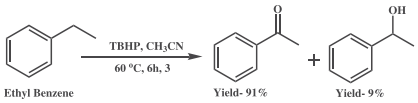

SCHEME 6 Oxidation of ethyl benzene catalyzed by **3**

detection limit of **2** for His are 2.1×10^5 M^{-1} and 0.23×10^{-7} M (Figure S25–26, ESI) respectively.

3.4 | Catecholase like activity

The reactions of **1–3** with 3, 5-DTBC, a model substrate to monitor catecholase like activity are carried out in

TABLE 5 Effect of oxidant and temperature on ethyl benzene oxidation using **3** as catalyst

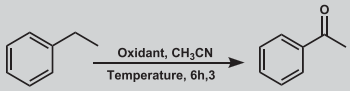

Entry	Oxidant	Temperature (°C)	Conversion (%)[a]	Yield[b] (%)	Selectivity of Acetophenone (%)[a]
1	**TBHP**	**60**	**86**	**72**	**91**
2	H_2O_2	60	67	42	59
3	PhIO	60	12	trace	trace
4	$NaIO_4$	60	27	10	19
5	$KHSO_5$	60	19	4	13
6	TBHP	50	52	23	60
7	TBHP	70	85	52	71

Reaction condition: 3 (10 mg), 10 mL acetonitrile, ethyl benzene (5 mmol), oxidant (10 mmol), reaction time, 6 h.
[a]determined by GC
[b]isolated yield.

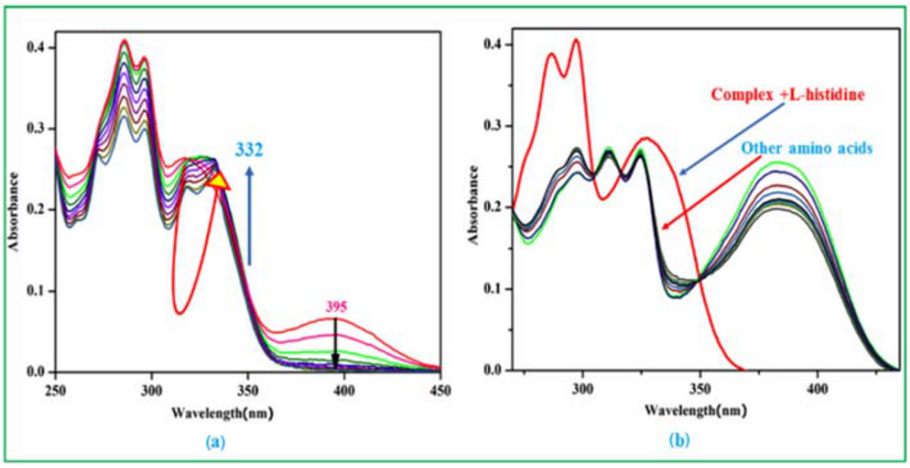

FIGURE 6 (a) Changes in the absorption spectra of **2**(10 μM) upon gradual addition of L-histidine (0–400 μM), (b) Absorption spectra of 2 (10 μM) in presence of different amino acids *viz.* (1) Methionine, (2) Argenine, (3) Valine, (4) Leucine, (5) Serine, (6) Lysine, (7) Trptophan, (8) Phenylalanyl, (9) Glycine, (10) Glutamic acid, (11) Glutamine, (12) Proline, (13) Iso-leucine, (14) Asparagine, (15) Aspartic acid, (16) Tyrsosine, (17) Threonine, (18) Cystine and (19) Alanine (other amino acids); Media: MeOH–water, 9: 1, *v*/v, 0.1 M HEPES buffer, pH 7.4

SCHEME 7 Proposed mechanism of Histidine sensing by **2**

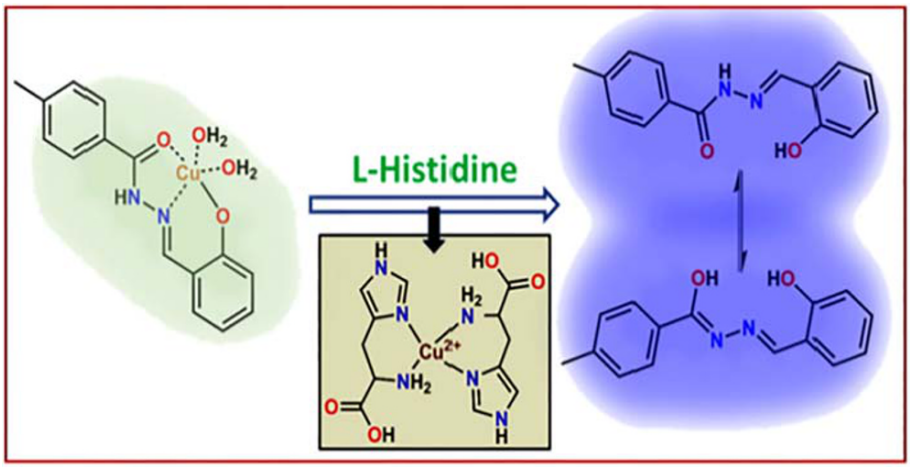

methanol by time dependent absorption spectroscopy. Thus, 1×10^{-4} mol dm^{-3} solution of **1–3** are treated with 1×10^{-2} mol dm^{-3} (100 equiv.) of 3, 5-DTBC under aerobic condition whereby a new peak at 392 nm, characteristics of 3, 5-di-*tert*-butyl benzoquinone (3, 5-DTBQ) appeared (Figure S27, ESI). In case of **3**, the peak for 3, 5-DTBQ appeared at 409 nm (Figure S27, ESI). Since initial rate method follows saturation kinetics at higher substrate concentration, Michaelis–Menten model for enzyme kinetics and corresponding Lineweaver-Burk plot allows determination of several kinetic parameters. Thus the binding constant (K_m), maximum velocity (V_{max}), and rate constant (turnover number, Kcat) are evaluated from Lineweaver–Burk plot, 1/V *vs.* 1/[S] using the equation $1/V = \{K_m/V_{max}\} \times \{1/[S]\} + 1/V_{max}$ (Figure 8, Table 6). The molecular ion peak at m/z, 562.65 in the ESI-MS^+ spectrum of the mixture of **1** and 3,5-DTBC indicates a 1: 1 (mole ratio, Figure S28, ESI). The peaks at m/z, 243.36 and 464.73 have been assigned to $[DTBQ\text{-}Na]^+$ and free metal complex respectively. Similarly, for **2**, the mass spectrum of the corresponding 1: 1 (mole ratio) adduct shows peak at m/z, 587.88. The other peaks at m/z 243.36, 413.64 and 464.73 have been assigned to $[DTBQ\text{-}Na]^+$ and free complex respectively (Figure S29, ESI). The mass spectrum (Figure S30, ESI) of 1: 1 (mole ratio) adduct between 3,5-DTBC and **3** have corresponding molecular ion peaks at m/z 633.88 and 668.03. The peaks at m/z 243.36 and 413.64 have been assigned to $[DTBQ\text{-}Na]^+$ and free complex respectively.

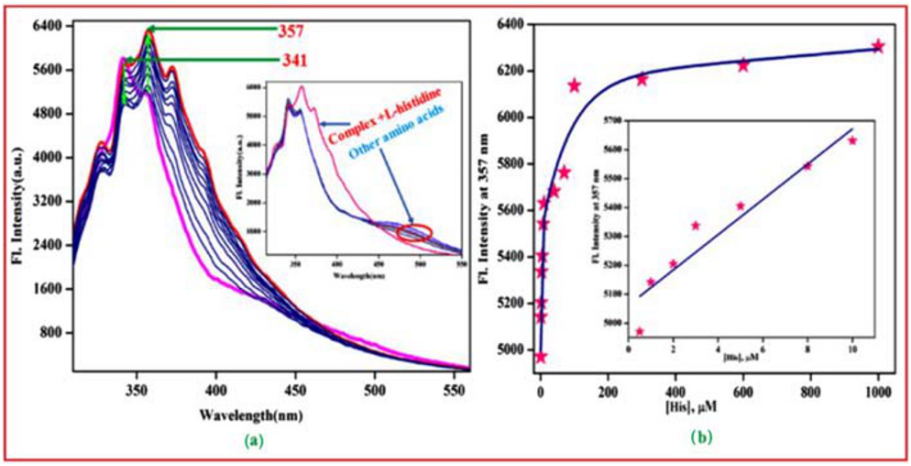

FIGURE 7 (a) Changes in the emission spectra of **2** (10 μM, λ_{ex}, 297 nm, λ_{em}, 357 nm) upon gradual addition of Histidine (0–400 μM); Inset: emission spectra of **2** (10 μM) in presence of different amino acid; (b) emission intensities of **2** *vs.* added His concentration; Inset: linear region of the plot

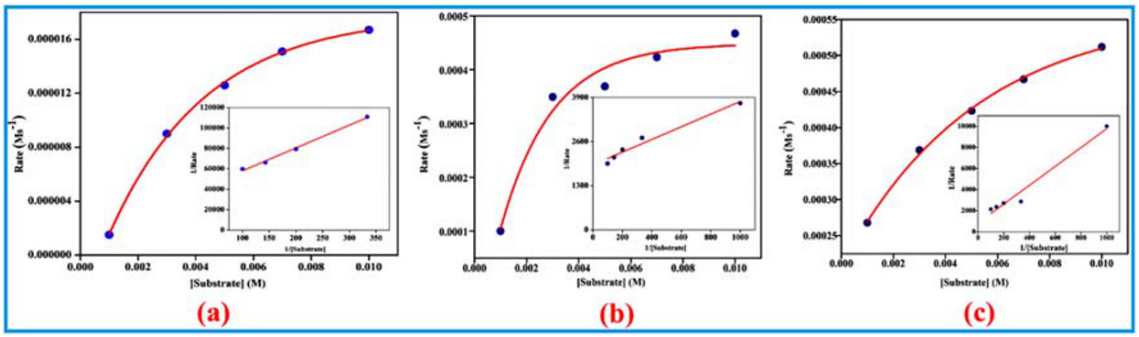

FIGURE 8 The plot of rate *vs.* substrate concentration using (a) **1**, (b) **2** and (c) **3** as catalyst. Inset: Lineweaver–Burk plot

TABLE 6 Kinetic parameters associated with catecholase like activity of **1**, **2** and **3**

Complex	V_{max} (Ms^{-1})	K_m (M)	K_{cat} (h^{-1})
1	2.79×10^{-5}	6.20×10^{-4}	1.00×10^{3}
2	1.10×10^{-3}	9.8×10^{-3}	35.3×10^{3}
3	5.2×10^{-4}	9.6×10^{-4}	18.7×10^{3}

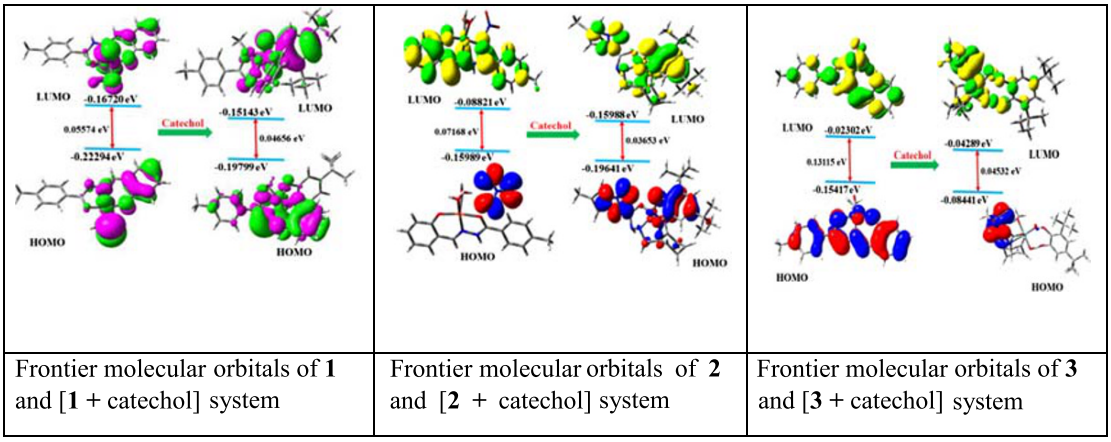

Frontier molecular orbitals of **1** and [**1** + catechol] system	Frontier molecular orbitals of **2** and [**2** + catechol] system	Frontier molecular orbitals of **3** and [**3** + catechol] system

FIGURE 9 **a** Frontier molecular orbitals of **1** and [**1** + catechol] system. **b** Frontier molecular orbitals of **2** and [**2** + catechol] system. **c** Frontier molecular orbitals of **3** and [**3** + catechol] system

3.5 | TD-DFT studies on complex-catechol interaction

The molecular level interaction of metal complexes, *viz.* **1**, **2** and **3** with catechol is studied by density functional theory (DFT) using B3LYP functional, 6-31G and lanl2mb basis sets. In general, HOMO and LUMO energy levels is lowered in catechol bound state. Thus, overall HOMO-LUMO energy gap decreases from 0.05574 eV to 0.04656 eV for **1**, 0.07168 eV to 0.03653 eV for **2** and 0.13115 eV to 0.04552 eV for **3** (Figure 9). Calculated transition energies for prominent absorption bands are presented in Table S4-S9 (ESI). The calculated absorption peaks agree well with the experimental peaks. The optimized structure of the respective complexes are shown in Figure S31 (ESI).

4 | CONCLUSIONS

Hydrazide based amide-amine conjugate $\mathbf{H_2L^{PTASAL}}$ and its Fe (III), Mo (VI) and Cu (II) complexes *viz.* **1**, **2** and **3** respectively were synthesized. SC-XRD characterized complexes were employed as catalyst for amine assisted epoxide ring opening, ethyl benzene oxidation and aryl-sulphur coupling reactions. Besides, catechol oxidase like properties of the complexes has also been tested and supported through DFT studies. In addition, the Cu (II) complex (**3**) selectively recognizes histidine by fluorescence spectroscopy.

ACKNOWLEDGMENTS

N.S acknowledge UGC, New Delhi for D. S Kothari Post-doctoral Fellowship (Award letter no. F.4-2/2006(BSR)/

CH/17-18/0176). The crystallographic studies were supported by the project CICECO – Aveiro Institute of Materials (UIDB/50011/2020 & UIDP/50011/2020), financed by National Funds through the FCT/MEC and co-financed by QREN-FEDER through COMPETE under the PT2020 Partnership Agreement.

CONFLICT OF INTEREST

There are no conflicts of interest to declare.

AUTHOR INFORMATION

Department of Chemistry, The University of Burdwan, Golapbag, Burdwan, India, Fax: +91–342-2,530,452; Tel: +91–342-2,533,913 (ext. 424); Email: ddas100in@yahoo.com

ORCID

Manirul Islam https://orcid.org/0000-0002-3970-5468
Debasis Das https://orcid.org/0000-0003-0474-0842

REFERENCES

[1] X. Liu, L. Lin, X. Feng, *Chem. Commun.* **2009**, *0*, 6145.
[2] a) M. Suzuki, H. Furutachi, H. Okawa, *Coord. Chem. Rev.* **2000**, *200*, 105. b) P. A. Vigato, S. Tamburini, *Coord. Chem. Rev.* **2004**, *248*, 1717. c) M. Andruh, *Chem. Commun.* **2011**, *47*, 3025. d) C. T. Lyons, T. D. P. Stack, *Coord. Chem. Rev.* **2013**, *257*, 528.
[3] K. Sone, Y. Fukuda, *Inorganic Chemistry Concept*, Vol. 10, Springer-Verlag, Heidelberg **1987** 43.
[4] S. Naskar, D. Mishra, M. Corbella, A. J. Blake, S. K. Chattopadhyay, *Dalton Trans.* **2005**, *0*, 2428.
[5] S. Naskar, M. Corbella, A. J. Blake, S. K. Chattopadhyay, *Dalton Trans.* **2007**, *0*, 1150.
[6] S. Naskar, D. Mishra, R. J. Butcher, S. K. Chattopadhyay, *Polyhedron* **2007**, *26*, 3703.
[7] a) L. H. Uppadine, J. P. Gisselbrecht, J. M. Lehn, *Chem. Commun.* **2004**, *0*, 718. b) L. H. Uppadine, J. M. Lehn, *Angew. Chem. Int. Ed.* **2004**, *43*, 240. c) M. Ruben, J. M. Lehn, G. Vaughan, *Chem. Commun.* **2003**, *0*, 1338. d) M. Prabhakar, P. S. Zacharias, S. K. Das, *Inorg. Chem.* **2005**, *44*, 2585. e) Z. He, C. He, E. Q. Gao, Z. M. Wang, X. F. Yang, C. S. Liao, C. H. Yan, *Inorg. Chem.* **2003**, *42*, 2206. f) S. Mondal, C. Das, B. Ghosh, B. Pakhira, A. J. Blake, M. G. B. Drew, S. K. Chattopadhyay, *Polyhedron* **2014**, *80*, 272. g) K. K. Bedia, O. Elçin, U. Seda, K. Fatma, S. Nathaly, R. A. Sevim, A. Dimoglo, *Eur. J. Med. Chem.* **2006**, *41*, 1253.
[8] a) P. Melnyk, V. Leroux, C. Sergheraert, P. Grellier, C. Sergheraert, *Bioorg. Med. Chem. Lett.* **2006**, *16*, 31. b) A. C. Cunha, J. M. Figueiredo, J. L. Tributino, A. L. Miranda, H. C. Castro, R. B. Zingali, C. A. Fraga, M. C. de Souza, V. F. Ferreira, E. J. Barreiro, *Med. Chem.* **2003**, *11*, 2051. c) L. Savanini, L. Chiasserini, A. Gaeta, C. Pellerano, *Bioorg. Med. Chem.* **2002**, *10*, 2193. d) H. Elo, P. Lumme, *Inorg. Chim. Acta* **1987**, *136*, 149.
[9] a) S. Hashiguchi, A. Kawada, H. Natsugari, *J. Chem. Soc. Perkin Trans.* **1991**, *0*, 2435. b) S. Knapp, *Chem. Rev.* **1995**, *95*, 1859. c) S. Horri, H. Fukase, T. Matsuo, Y. Kameda, N. Asano, K. Matsui, *J. Med. Chem.* **1986**, *29*, 1038. d) D. J. Ager, I. Prakash, D. R. Schaad, *Chem. Rev.* **1996**, *96*, 835.
[10] a) M. D. McReynolds, J. M. Dougherty, *Chem. Rev.* **2004**, *104*, 2239. b) I. P. Beletskaya, V. P. Ananikov, *Chem. Rev.* **2011**, *111*, 1596.
[11] a) A. Gangjee, F. Mavandadi, R. L. Kisliuk, J. J. McGuire, S. F. Queener, *J. Med. Chem.* **2007**, *50*, 3046. b) G. De Martino, G. L. Regina, A. Coluccia, M. C. Edler, M. C. Barbera, A. Brancale, E. Wilcox, E. Hamel, M. Artico, R. Silvestri, *J. Med. Chem.* **2004**, *47*, 6120.
[12] I. P. Beletskaya, A. V. Cheprakov, *Coord. Chem. Rev.* **2004**, *248*, 2337.
[13] T. Kondo, T. A. Mitsudo, *Chem. Rev.* **2000**, *100*, 3205.
[14] a) S. V. Ley, A. W. Thomas, *Angew. Chem. Int. Ed.* **2003**, *42*, 5400. b) I. P. Beletskaya, A. V. Cheprakov, *Coord. Chem. Rev.* **2004**, *248*, 2337. c) S. R. Hemler, P. H. Fuller, *Chem. Soc. Rev.* **2007**, *36*, 1153. d) G. Evano, N. Blanchard, M. Toumi, *Chem. Rev.* **2008**, *108*, 3054. e) I. P. Beletskaya, V. P. Ananikov, *Chem. Rev.* **2011**, *111*, 1596.
[15] W. Q. Zhang, A. J. Atkin, I. J. Fairlamb, A. C. Whitwood, J. M. Lynam, *Organometallics* **2011**, *30*, 4643.
[16] M. R. Maurya, S. Dhaka, F. Avecilla, *Polyhedron* **2014**, *67*, 145.
[17] a) L. Yang, R. McRae, M. M. Henary, R. Patel, B. Lai, S. Vogt, C. Fahrni, *Proc. Natl. Acad. Sci. U. S. a.* **2005**, *102*, 11179. b) M. Lopez-Alonso, M. Miranda, J. L. Benedito, V. Pereira, M. Garcı'a-Vaquero, *Meat Sci.* **2016**, *121*, 47.
[18] a) T. Hirayama, G. C. Van de Bittner, L. W. Gray, S. Lutsenko, C. Chang, *Proc. Natl. Acad. Sci. U. S. a.* **2012**, *109*, 2228. b) A. Raab, J. Nelson, M. Stiboller, P. Franzmann, Z. Gajdosechova, J. Feldmann, *Planta Med.* **2016**, *82*, OA39.
[19] a) H. Tapiero, D. M. Townsend, K. D. Tew, *Copper. Biomed. Pharmacol. J.* **2003**, *57*, 386. b) T. C. B. Pereira, M. M. Camposa, M. R. Bogo, *J. Appl. Toxicol.* **2016**, *36*, 876.
[20] B. Halliwell, J. M. Gutteridge, *J. Biochem.* **1984**, *219*, 1.
[21] J. D. Gitlin, *Gastroenterology* **2003**, *125*, 1868.
[22] J. F. B. Mercer, *Trends Mol. Med.* **2001**, *7*, 64.
[23] G. Multhaup, A. Schlicksupp, L. Hesse, D. Beher, T. Ruppert, C. L. Masters, K. Beyreuther, *Science* **1996**, *271*, 1406.
[24] D. J. Waggoner, T. B. Bartnikas, J. D. Gitlin, *Neurobiol. Dis.* **1999**, *6*, 221.
[25] F. Lebon, N. Boggetto, M. Ledecq, *Biochem. Pharmacol.* **2002**, *63*, 1863.
[26] B. Kumari, S. Kundu, K. Ghosh, M. Banerjee, S. K. Pradhan, S. K. M. Islam, P. Brandao, V. Felix, D. Das, *Dalton Trans* **2018**, *47*, 14008.
[27] Y. Zhou, J. Won, J. Y. Lee, J. Yoon, *Chem. Commun.* **2011**, *47*, 1997.
[28] Z. Li, X. Lou, Z. Li, J. A. Qin, *ACS Appl. Mater. Interfaces* **2009**, *2*, 232.
[29] Y. Zhou, J. Yoon, *Chem. Soc. Rev.* **2012**, *41*, 52.
[30] a) J. D. Kopple, M. E. Swendseid, *J. Clin. Invest.* **1975**, *55*, 881. b) S. E. Snyderman, A. Boyer, E. Roitman, L. E. Holt, P. H. Prose Jr., *Pediatrics.* **1963**, *31*, 786. c) Y. Kusakari,

S. Nishikawa, S. Ishiguro, M. Tamai, *Curr. Eye Res.* **1997**, *16*, 600.
[31] M. Watanabe, M. E. Suliman, A. R. Qureshi, E. Garcia-Lopez, P. Barany, O. Heimburger, P. Stenvinkel, B. Lindholm, *Am. J. Clin. Nutr.* **2008**, *87*, 1860.
[32] a) A. L. Jones, M. D. Hulett, C. R. Parish, *Immunol. Cell Biol.* **2005**, *83*, 106. b) D. J. Sullivan Jr., I. Y. Gluzman, D. E. Goldberg, *Science* **1996**, *271*, 219. c) F. W. G. Leebeek, C. Kluft, E. A. R. Knot, M. P. M. De, *Lab. Clin. Med.* **1989**, *113*, 493. d) H. Saito, L. T. Goodnough, J. M. Boyle, N. Heimburger, *Am. J. Med.* **1982**, *73*, 179.
[33] a) M. A. Hortala, L. Fabbrizzi, N. Marcotte, F. Stomeo, A. Taglietti, *J. Am. Chem. Soc.* **2003**, *125*, 20. b) L. Fabbrizzi, G. Francese, M. Licchelli, A. Perotti, A. Taglietti, *Chem. Commun.* **1997**, *0*, 581. c) D.-L. Ma, W.-L. Wong, W.-H. Chung, F.-Y. Chan, P.-K. So, T.-S. Lai, Z.-Y. Zhou, Y.-C. Leung, K.-Y. Wong, *Angew. Chem. Int. Ed.* **2008**, *47*, 3735. d) Y. Zhang, R. H. Yang, F. Liu, K.-A. Li, *Anal. Chem.* **2004**, *76*, 7336. e) Y.-Y. Fu, H.-X. Li, W.-P. Hu, *Sens. Actuators, B* **2008**, *131*, 167.
[34] a) J. F. Folmer-Andersen, V. M. Lynch, E. V. Anslyn, *Chem. – Eur. J.* **2005**, *11*, 5319. b) Y. Y. Liu, M. G. Fan, S. X. Zhang, X. H. Sheng, J. N. Yao, *New J. Chem.* **2007**, *31*, 1878. c) P. Wu, X.-P. Yan, *Biosens. Bioelectron.* **2010**, *26*, 485. d) C. C. Huang, W. L. Tseng, *Analyst* **2009**, *134*, 1699. e) X. Li, H. Ma, L. Nie, M. Sun, X. Xiong, *Anal. Chim. Acta* **2004**, *515*, 255. (f) Z. Zhang, H. Liao, H. Li, L. Nie, S. Yao, *Anal. Biochem.* **2005**, *336*, 108.
[35] a) A. W. Czarnik, *Chem. Biol.* **1995**, *2*, 423. b) E. K. Feuster, T. E. Glass, *J. Am. Chem. Soc.* **2003**, *125*, 16174. c) S. Pagliari, R. Corrandini, G. Galaverna, S. Sforza, A. Dossena, M. Montalti, L. Prodi, N. Zaccheroni, R. Marchelli, *Chem. – Eur. J.* **2004**, *10*, 2749. d) A. T. Wright, E. V. Anslyn, *Org. Lett.* **2004**, *6*, 1341. e) J. S. You, X. Q. Yu, G. L. Zhang, Q. X. Xiang, J. B. Lan, R. G. Xie, *Chem. Commun.* **2001**, *0*, 1816. f) W. L. Wong, K. A. Huang, P. F. Teng, C. S. Lee, H. L. Kwong, *Chem. Commun.* **2004**, *0*, 384. g) J. W. Canary, A. E. Holmes, J. Liu, *Enantiomer* **2001**, *6*, 181.
[36] Z. Huang, J. Du, J. Zhang, X.-Q. Yu, L. Pu, *Chem. Commun.* **2012**, *48*, 3412.
[37] S. J. Dixon, B. R. Stockwell, *Nat. Chem. Biol.* **2014**, *10*, 9.
[38] R. S. Eisenstein, *Annu. Rev. Nutr.* **2000**, *20*, 627.
[39] B. F. Matzanke, G. Muller-Matzanke, K.N. Raymond, VCH Publishers, New York, **1989**.
[40] N. C. Andrews, *N. Engl. J. Med.* **1999**, *341*, 1986.
[41] D. Touati, *Arch. Biochem. Biophys.* **2000**, *373*, 1.
[42] E. Beutler, V. Felitti, T. Gelbart, N. Ho, *Drug Metab. Dispos.* **2001**, *29*, 495.
[43] R. R. Crichton, *2nd edn*, John Wiley & Sons, Chichester **2001**.
[44] G. Tangen, T. Wickstrøm, S. Lierhagen, R. Vogt, W. Lund, *Environ. Sci. Technol.* **2002**, *36*, 5421.
[45] a) S. Dasgupta, J. Adhikary, S. Giri, A. Bauza, A. Frontera, D. Das, *Dalton Trans.* **2017**, *46*, 5888. b) P. Adak, B. Ghosh, A. Bauza, A. Frontera, A. J. Blake, M. Corbella, C. D. Mukhopadhyaye, S. K. Chattopadhyaya, *RSC Adv.* **2016**, *6*, 86851. c) S. Adhikari, A. Banerjee, S. Nandi, M. Fondo, J. Sanmartin-Matalobos, D. Das, *RSC Adv.* **2015**, *5*, 10987. d) P. Mahapatra, S. Ghosh, S. Giri, V. Rane, R. Kadam, M. G. B. Drew, A. Ghosh, *Inorg. Chem.* **2017**, *56*, 5105.
[46] a) X. L. Hou, J. Wu, L. X. Dai, L.-J. Xia, M. H. Tang, *Tetrahedron: Asymmetry* **1998**, *9*, 1747. b) S. Sagawa, H. Abe, Y. Hase, T. Inaba, *J. Org. Chem.* **1999**, *64*, 4962. c) G. Bartoli, M. Bosco, A. Carlone, M. Locatelli, M. Massaccesi, P. Melchiorreand, L. Sambri, *Org. Lett.* **2004**, *6*, 2173.
[47] a) F. Carree, R. Gil, J. Collin, *Org. Lett.* **2005**, *7*, 1023. b) S. Azoulay, K. Manabe, S. Kobayashi, *Org. Lett.* **2005**, *7*, 4593. c) K. Arai, M. M. Salter, Y. Yamashita, S. Kobayashi, *Angew. Chem. Int. Ed.* **2007**, *46*, 955. d) E. Mai, C. Schneider, *Chem. – Eur. J.* **2007**, *13*, 2729.
[48] a) K. Arai, S. Lucarini, M. M. Salter, K. Ohta, Y. Yamashita, S. Kobayashi, *J. Am. Chem. Soc.* **2007**, *129*, 8103. b) E. Mai, C. Schneider, *Synlett* **2007**, *13*, 2136. c) H. Bao, J. Zhou, Z. Wang, Y. Guo, T. You, K. Ding, *J. Am. Chem. Soc.* **2008**, *130*, 10116. d) B. Gao, Y. Wen, Z. Yang, X. Huang, X. Liu, X. Feng, *Adv. Synth. Catal.* **2008**, *350*, 385. e) H. Bao, J. Wu, H. Li, Z. Wang, T. You, K. Ding, *Eur. J. Org. Chem.* **2010**, *2010*, 6722. f) M. Martin, A. El Hellani, J. Yang, J. Collin, *J. Org. Chem* **2011**, *76*, 9801.
[49] M. C. Burla, R. Caliandro, M. Camalli, B. Carrozzini, G. L. Cascarano, L. De Caro, C. Giacovazzo, G. Polidori, R. Spagna, *J. Appl. Crystallogr.* **2005**, *38*, 381.
[50] G. M. Sheldrick, *Acta Crys.* **2015**, *A71*, 3.
[51] G. M. Sheldrick, *Acta Cryst.* **2015**, *C71*, 3.
[52] C. F. Macrae, I. J. Bruno, J. A. Chisholm, P. R. Edgington, P. McCabe, E. Pidcock, L. R. Rodriguez-MongeTaylor, J. van de Streek, P. A. Wood, *J. Appl. Crystallogr.* **2008**, *41*, 466.
[53] The PyMOL, Version 2.0 Schrödinger, Molecular Graphics System, LLC.
[54] (a) S. Zuffanti, *J. Chem. Educ.* **1948**, *25*, 481. b) B. K. Datta, D. Thiyagarajan, A. Ramesh, G. Das, *Dalton Trans.* **2015**, *44*, 13093.
[55] A. Pal, B. Biswas, S. K. Mondal, C.-H. Lin, R. Ghosh, *Polyhedron* **2012**, *31*, 671.
[56] R. Dinda, P. Sengupta, S. Ghosh, W. S. Sheldrick, *Eur. J. Inorg. Chem.* **2003**, *2003*, 363.
[57] V. Vrdoljak, M. Cindri, D. Matkovic-Calogovi, B. Prugovecki, P. Novak, B. Kamenar, *Z. Anorg. Allg. Chem.* **2005**, *631*, 928.
[58] a) A. B. Khudoyarov, Kh.T. Sharipov, M. A. Porai-Koshits, **1987**. b) K. Khim, *Coord.Chem.* **2010**, *13*, 269.
[59] T. Ollevier, *Catal. Sci. Technol.* **2016**, *6*, 41.

SUPPORTING INFORMATION

Additional supporting information may be found online in the Supporting Information section at the end of this article.

How to cite this article: Ta S, Ghosh M, Salam N, et al. X-ray structurally characterized Mo (VI), Fe (III) and Cu (II) complexes of amide-imine conjugate: (bio)catalytic and histidine recognition studies. *Appl Organomet Chem*. 2020;e5823. https://doi.org/10.1002/aoc.5823